

# Shear dispersion of multispecies electrolyte solutions in channel domain

Lingyun Ding<sup>1†</sup>

<sup>1</sup>Department of Mathematics, University of California Los Angeles, CA, 90095, United States

(Received xx; revised xx; accepted xx)

In multispecies electrolyte solutions, even in the absence of an external electric field, differences in ion diffusivities induce an electric potential and generate additional fluxes for each species. This electro-diffusion process is well-described by the advection-Nernst-Planck equation. This study aims to analyze the long-time behavior of the governing equation under the electroneutrality and zero current conditions and investigate how the diffusion-induced electric potential and the shear flow enhance the effective diffusion coefficients of each species in channel domains. To achieve this goal, the homogenization method was used to derive a reduced model of the advection-Nernst-Planck equation in the channel domain. There are several interesting properties of the effective equation. First, it is a generalization of the Taylor dispersion, with a nonlinear diffusion tensor replacing the scalar diffusion coefficient. Second, the effective equation reveals that the system without the flow is asymptotically equivalent to the system with a strong flow and scaled physical parameters. Furthermore, when the background concentration is much greater than the perturbed concentration, the effective equation reduces to a multidimensional diffusion equation, consistent with the classical Taylor dispersion theory. However, for zero background concentration, the ion-electric interaction results in several phenomena don't present in the advection-diffusion equation, including upstream migration of some species, spontaneous separation of ions, and non-monotonic dependence of the effective diffusivity on Péclet numbers. Last, the dependence of effective diffusivity on concentration and ion diffusivity suggests a method to infer the concentration ratio of each component and ion diffusivity by measuring the effective diffusivity.

**Key words:** Diffusion coefficient, Multispecies electrolyte solution, Nernst-Planck equation, Taylor dispersion

## 1. Introduction

Fluid flow plays an important role in the transport of solutes. When a solute is transported in a fluid through a narrow tube or channel, the interaction of fluid flow and molecular diffusion causes the solute to spread out and become more dispersed as it travels down the tube. This effect is known as Taylor dispersion, named after G. I. Taylor, who first investigated the phenomenon in Taylor (1953). Since Taylor's seminal work, theoretical studies on Taylor dispersion have expanded and exploded in many directions (Aris (1956, 1960); Chatwin (1970); Vedel & Bruus (2012); Ding & McLaughlin (2021)), and established applications in many disciplines such as molecular diffusivity

---

† Email address for correspondence: dingly@ucla.edu

measurement (Bello *et al.* (1994); Taladriz-Blanco *et al.* (2019); Leaist (2017)), chemical delivery in micro-channel (Aminian *et al.* (2016); Dutta & Leighton (2001)), contaminant dispersion (Chatwin (1975); Smith (1982); Ngo-Cong *et al.* (2015)).

In an electrolyte solution, the electric current is carried by the dissolved ions. The electric field exerts significant body forces on the ions, affecting their fluxes, which is another key factor in mass transfer. Even in the absence of an external electric field, where the electroneutrality and zero current conditions are met, it is necessary to consider ion-electric interaction in multispecies electrolyte solutions because dissolved ions have different diffusivities. To maintain electroneutrality, the faster-moving ion is slowed down, creating a balance between positive and negative charges. For example, sodium fluorescein is a commonly used tracer in fluid experiments, and its self-diffusion coefficient in water has been measured experimentally by several authors to be around  $4 \sim 5 \times 10^{-6} \text{ cm}^2\text{s}^{-1}$  (Casalini *et al.* (2011)). However, given the fact that the sodium ion has a larger diffusivity of  $15 \times 10^{-6} \text{ cm}^2\text{s}^{-1}$  (Smith & Sansom (1998)), when sodium fluorescein is in a sodium chloride stratified fluid, the sodium ions from the sodium chloride can boost its diffusion coefficient to  $8 \sim 9 \times 10^{-6} \text{ cm}^2\text{s}^{-1}$  (Ding *et al.* (2021)).

The system involves fluid flow, electric field, and diffusion can be well-described by the advection-Nernst-Planck equation (Deen (1998); Maex (2013)). Many recent studies show that the transport of multiple electrolytes exhibits different properties compared with the transport of a single binary electrolyte (Gupta *et al.* (2019); Hosokawa *et al.* (2011); Liu *et al.* (2011)). When dealing with two different ion species, the nonlinear governing equation can be reduced to the advection-diffusion equation (Deen (1998)), allowing for simplified analysis. However, when dealing with more than two different ion species, the complexity of the nonlinear governing equation prohibits simplification to the advection-diffusion equation, necessitating a comprehensive consideration of the electro-diffusive process to accurately describe the system's behavior.

Understanding how fluid flow, electric potential, and diffusion interact in multispecies electrolyte solutions is essential for accurately measuring mutual diffusion (Leaist & Hao (1993); Price (1988); Ribeiro *et al.* (2019); Rodrigo *et al.* (2022, 2021)), as well as for simulating the system with stratified fluids (Poisson & Papaud (1983); Ben-Yaakov (1972); Yuan-Hui & Gregory (1974); Ding *et al.* (2021)), and for controlling diffusio-phoresis (Ault *et al.* (2017)) and modeling isotachophoresis (Bhattacharyya *et al.* (2013); Gopmandal & Bhattacharyya (2015); GanOr *et al.* (2015)). Despite its importance, the interplay between these three factors has not been extensively studied in the literature, creating a knowledge gap. The main goal of this study is to fill this gap by presenting a comprehensive investigation of this interplay.

To this end, we use homogenization methods to derive an effective equation that is valid at the diffusion time scale for the advection-Nernst-Planck equation in a channel with arbitrary cross-sectional geometry. In addition, the resulting effective equation depends only on the longitudinal variable of the channel, and provides a more tractable approximation for analyzing mass transfer which captures the combined effects of flow advection and ion-electric interaction.

Our analytical results show that the variance of the concentration distribution asymptotically increases linearly with time, and we demonstrate that the effective diffusivity can be efficiently calculated via the self-similar solution of the effective equation. Effective diffusivity is a critical parameter for understanding the mass transfer and guiding the designing of microfluidic devices (Dutta & Leighton (2001)), and we show that it can also be used to infer the concentration ratio of each component and ion diffusivity in multispecies electrolyte solutions. We demonstrate that the effective equation exhibits a reciprocal property, namely, the system without flow is mathematically equivalent to the

system with a strong flow and scaled physical parameters. Moreover, we find that the nonlinear effective equation can be approximated by a diffusion equation with mutual diffusion coefficients when the background concentration is nonzero.

To complement our analytical results, we conduct numerical simulations to explore the behavior of multispecies electrolyte solutions under different flow and electric field conditions, validating our analytical results. Our simulations reveal several interesting properties arising from the nonlinearity of the advection-Nernst-Planck equation, such as upstream migration of some species, separation of ions depending on the flow strength, the presence of highly non-Gaussian and bimodal shape of concentration distribution and a non-monotonic dependence of the effective diffusivity on Péclet numbers.

The paper is structured as follows. In Section 2, we present the governing equations for the transport of multispecies electrolyte solutions in channel domains and review the definition of effective diffusivity. In Section 3, we derive the effective equation of the advection-Nernst-Planck equation at long times using homogenization methods, and compare the result with that of Taylor dispersion. In Section 4, we validate our analytical results with numerical simulations and explore interesting phenomena arising from the ion-electric interaction. In Section 5, we summarize our findings and discuss future research directions. Appendix A presents the effective equation for some shear flows in the parallel-plate channel domain and circular pipe.

## 2. Governing equation and effective diffusivity

### 2.1. Advection-Nernst-Planck equation

Denote the concentration and valence of  $i$ -th species of ion as  $c_i(x, t)$  and  $z_i$ , respectively. The concentration evolution of  $n$  ion species under the shear flow advection and ionic interaction can be modeled by the Nernst-Planck equation (see section 11.7 in Deen (1998), or Maex (2013)),

$$\begin{aligned} \partial_t c_i + u(\mathbf{y}, t) \partial_x c_i &= \kappa_i \Delta c_i + \frac{\kappa_i z_i e}{k_b T} \nabla \cdot (c_i \nabla \phi), \\ c_i(x, \mathbf{y}, 0) &= c_{I,i} \left( \frac{x}{L_x} \right), \quad \mathbf{n} \cdot \nabla c_i|_{\mathbb{R} \times \partial\Omega} = 0, \quad i = 1, \dots, n, \end{aligned} \quad (2.1)$$

where  $\kappa_i$  is the diffusivity of the  $i$ -th species of ion,  $\phi$  is the electric potential,  $e$  is the charge of an electron,  $k_b$  is the Boltzmann constant and  $T$  is the temperature.  $u(\mathbf{y}, t)$  is a periodic time-varying function with a period  $L_t$ . Based on the physical meaning,  $c_i$  is non-negative for all  $x, \mathbf{y}$  and  $t$ .

The channel domain is  $(x, \mathbf{y}) \in \mathbb{R} \times \Omega$ , where the  $x$ -direction is the longitudinal direction of the channel and  $\Omega \subset \mathbb{R}^d$  stands for the cross-section of the channel.  $\mathbf{n}$  is the outward normal vector of the boundary,  $\mathbb{R} \times \partial\Omega$ , where  $\partial\Omega$  is the boundary of  $\Omega$ . Some practical examples of the channel boundary geometry includes the parallel-plate channel  $\Omega = \{y|y \in [0, L_y]\}$  (sketched in figure 1), the circular pipe  $\Omega = \{\mathbf{y}|\mathbf{y}^2 \leq L_y^2\}$ , the rectangular duct  $\Omega = \{\mathbf{y}|\mathbf{y} \in [0, L_y] \times [0, H_y]\}$ , and bowed rectangular channels (Lee *et al.* (2021)). For the detailed procedure and setup of the channel flow experiments, we refer to the article Aminian *et al.* (2018). In this study, we assume that the characteristic length scale  $L_x$  of the initial condition  $c_{I,i}$  is much larger than the characteristic length scale of the channel cross-section  $L_y$ . This assumption is commonly known as the slow varying assumption in the literature (see, for example, Camassa *et al.* (2010)).

Now there are  $n$  conservation equations for  $n$  concentration fields and an unknown electric potential  $\phi$ . An additional equation is furnished by the electroneutrality condition

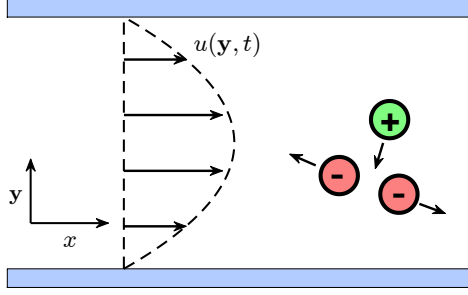


FIGURE 1. The schematic shows the setup for the special case of a quadratic shear flow in the parallel-plate channel domain. A multispecies electrolyte in water exists in the form of dissolved ions. Ions of like charges repel, while ions of opposite charges attract, due to electrostatic forces. The interplay between the flow and the ion-electric interactions plays a crucial role in determining the behavior and dynamics of the system.

$\sum_{i=1}^n z_i c_i = 0$ . In the absence of an external electric field, the zero electric current condition is a reasonable assumption,  $0 = \sum_{i=1}^n z_i J_i = \sum_{i=1}^n z_i \left( u \begin{bmatrix} c_i \\ \mathbf{0} \end{bmatrix} - \kappa_i \nabla c_i - \frac{\kappa_i z_i e}{k_b T} c_i \nabla \phi \right)$ , which is used in many literature (Ben-Yaakov (1972); Tournassat *et al.* (2020); Gupta *et al.* (2019); Tabrizinejadas *et al.* (2021)). Moreover, for the electroneutrality initial data, the zero electric current condition ensures that the electroneutrality condition is always true (see Boudreau *et al.* (2004)). Using the zero electric current condition, the electric potential can be expressed in terms of ion concentrations

$$\frac{e}{k_b T} \nabla \phi = \frac{\sum_{i=1}^n z_i \left( u \begin{bmatrix} c_i \\ \mathbf{0} \end{bmatrix} - \kappa_i \nabla c_i \right)}{\sum_{i=1}^n z_i^2 \kappa_i c_i} = \frac{\sum_{i=1}^{n-1} (\kappa_n - \kappa_i) z_i \nabla c_i}{\sum_{i=1}^{n-1} (z_i \kappa_i - z_n \kappa_n) z_i c_i}, \quad (2.2)$$

where the second step follows the electroneutrality condition. Equation (2.2) shows that the electric potential gradient is induced by the difference in ion diffusivities. When all diffusivities take the same value, the gradient of the diffusion-induced potential becomes zero, and equation (2.1) reduces to the advection-diffusion equation. When there is a difference in diffusivities, substituting equation (2.2) into Nernst-Planck equation (2.1) yields the equation that will be mainly used in this study

$$\partial_t c_i + u(\mathbf{y}, t) \partial_x c_i = \kappa_i \Delta c_i + \kappa_i z_i \nabla \cdot \left( \frac{c_i \sum_{j=1}^{n-1} (\kappa_n - \kappa_j) z_j \nabla c_j}{\sum_{j=1}^{n-1} (z_j \kappa_j - z_n \kappa_n) z_j c_j} \right), \quad i = 1, \dots, n-1. \quad (2.3)$$

## 2.2. Effective diffusivity

As demonstrated by many studies (Taylor (1953); Aris (1956); Chatwin (1970); Ding & McLaughlin (2022)), the solution of the advection-diffusion equation in the channel domain converges to a Gaussian distribution function at long times. To model this behavior, one can use a diffusion equation with an enhanced effective diffusion coefficient. Therefore, understanding the dependence of the effective diffusion coefficient on the flow conditions, channel geometries, and ion physical parameters is important for optimizing

microfluidic device performance, either enhancing or reducing mixing (Dutta & Leighton (2001); Aminian *et al.* (2016, 2015)).

The precise definition of the effective diffusion coefficient depends on the initial condition. In this study, we consider three types of initial conditions. The first type of initial condition is an integrable function that vanishes at infinity, such as  $c_{I,i}(x) = \frac{2}{\sqrt{\pi}}e^{-x^2}$ . This type of initial condition can be used to model the delivery of chemicals with a finite volume in a capillary tube (see Aminian *et al.* (2016)). In the second type of initial condition, the concentration field can be expressed as  $c_i = c_i(\infty) + \tilde{c}_i$ , where  $c_i(\infty)$  is a constant representing the background concentration, and  $\tilde{c}_i$  is an integrable function representing the deviation from the background concentration, for example,  $c_{I,i}(x) = 1 + \frac{2}{\sqrt{\pi}}e^{-x^2}$ . In many experimental studies (e.g., Leaist & MacEwan (2001); Leaist (2017)), the pipe is filled with buffer solutions. In such cases,  $c_i(\infty) > 0$ , and  $\tilde{c}_i$  can take negative values as long as  $c_i$  remains non-negative. In the third type of initial condition, the concentration field tends to a constant value at infinity, but the values at positive and negative infinity can be different, such as  $c_{I,i}(x) = \text{erf}(x) = \frac{2}{\sqrt{\pi}} \int_0^x e^{-t^2} dt$ , which can be used to model the continuous injection of a solution with a constant concentration into the channel domain (see Taylor (1953)). The solutions of the equations with these three types of initial conditions exhibit different long-time asymptotic properties, and therefore we have treated them separately in our analysis.

For the first type of initial condition, the effective longitudinal effective diffusivity is given by

$$\kappa_{\text{eff}} = \lim_{t \rightarrow \infty} \frac{\text{Var}(\bar{c})}{2t \int_{-\infty}^{\infty} \bar{c} dx} = \lim_{t \rightarrow \infty} \frac{\partial_t \text{Var}(\bar{c})}{2 \int_{-\infty}^{\infty} \bar{c} dx}, \quad (2.4)$$

where  $\bar{c}(x, t) = \frac{1}{|\Omega|} \int_{\Omega} c(x, \mathbf{y}, t) d\mathbf{y}$  is the cross-sectional average of the scalar field.  $|\Omega|$  is

the area of  $\Omega$ .  $\text{Var}(\bar{c}) = \int_{-\infty}^{\infty} \bar{c} x^2 dx - \left( \int_{-\infty}^{\infty} \bar{c} x dx \right)^2$  is the variance of the cross-sectional averaged concentration field  $\bar{c}$ . In other words, the asymptotics of the variance is given by

$$\text{Var}(\bar{c}) \approx \text{Var}(\bar{c}_I) + 2t\kappa_{\text{eff}} \int_{-\infty}^{\infty} \bar{c} dx, \quad t \rightarrow \infty. \quad (2.5)$$

For the second type of initial condition, where the background ion concentration is nonzero,  $c_i$  is not integrable. One can define the effective longitudinal effective diffusivity via the perturbed concentration

$$\kappa_{\text{eff}} = \lim_{t \rightarrow \infty} \frac{\text{Var}(\bar{c} - c(\infty))}{2t \int_{-\infty}^{\infty} \bar{c} - c(\infty) dx} = \lim_{t \rightarrow \infty} \frac{\partial_t \text{Var}(\bar{c} - c(\infty))}{2 \int_{-\infty}^{\infty} \bar{c} - c(\infty) dx}. \quad (2.6)$$

The solution with the third of initial condition is also not integrable, but we can investigate its derivative,

$$\kappa_{\text{eff}} = \lim_{t \rightarrow \infty} \frac{\text{Var}(\partial_x \bar{c})}{2t(\bar{c}(\infty) - c(-\infty))} = \lim_{t \rightarrow \infty} \frac{\partial_t \text{Var}(\partial_x \bar{c})}{2(\bar{c}(\infty) - c(-\infty))}. \quad (2.7)$$

Although the diffusion-induced electric potential may cause the concentration field to deviate from a Gaussian distribution function, we are still interested in computing the effective diffusivity for several reasons. First, when the electric potential is weak and the

background concentration is nonzero, the solution can be reasonably approximated by a Gaussian distribution function or error function. Second, as the time approaches infinity, the variance  $\text{Var}(\bar{c})$  increases linearly, ensuring that the effective diffusivity remains well-defined quantity for characterizing the system. Third, by examining the relationship between effective diffusivity and other physical parameters, e.g., ion diffusivity, one can devise an experimental method for measuring the latter.

### 3. Effective equation

It is possible to develop a simplified model that depends only on the longitudinal variable and time, given that the length scale in the longitudinal direction of the channel domain is significantly larger than the length scale in the transverse direction. By simplifying the model in this way, one can reduce the computational complexity of the problem while retaining the relevant physical phenomena without compromising the key features of interest. The homogenization method is a widely used method to achieve this goal, especially for the linear advection-diffusion problem (Camassa *et al.* (2010); Wu & Chen (2014); Bronski *et al.* (2022)). Here, we will see that the homogenization method can yield the effective equation for the nonlinear equation (2.1).

#### 3.1. Homogenization method

The first step is to non-dimensionalize the equation, which helps identify the dominant terms. The change of variables for the nondimensionalization is

$$\begin{aligned} L_x x' = x, \quad L_y \mathbf{y}' = \mathbf{y}, \quad \epsilon = \frac{L_y}{L_x}, \quad \frac{L_y^2}{\tilde{\kappa} \epsilon^2} t' = t, \\ \tilde{c} c'_i = c_i, \quad \frac{e}{k_b T} \phi' = \phi, \quad U u' \left( \mathbf{y}', \frac{t'}{\epsilon^2} \right) = u(\mathbf{y}, t), \end{aligned} \quad (3.1)$$

where  $\tilde{c}$  is the characteristic concentration,  $\tilde{\kappa}$  is the characteristic diffusivity. One can drop the primes without confusion and obtain the non-dimensionalized equation,

$$\begin{aligned} \partial_t c_i + \frac{\text{Pe} u(\mathbf{y}, \frac{t}{\epsilon^2})}{\epsilon} \partial_x c_i &= \kappa_i \partial_x (\partial_x c_i + z_i c_i \partial_x \phi) + \frac{\kappa_i}{\epsilon^2} \nabla_{\mathbf{y}} \cdot (\nabla_{\mathbf{y}} c_i + z_i c_i \nabla_{\mathbf{y}} \phi), \\ c_i|_{t=0} &= c_{I,i}(x), \quad \mathbf{n} \cdot \nabla c_i|_{\mathbb{R} \times \partial \Omega} = 0, \quad i = 1, \dots, n-1, \\ \nabla \phi &= \frac{\sum_{i=1}^{n-1} (\kappa_n - \kappa_i) z_i \nabla c_i}{\sum_{i=1}^{n-1} (z_i \kappa_i - z_n \kappa_n) z_i c_i}, \end{aligned} \quad (3.2)$$

where  $\nabla_{\mathbf{y}} = (\partial_{y_1}, \dots, \partial_{y_d})$ ,  $\text{Pe} = \frac{L_y U}{\tilde{\kappa}}$  is the Péclet number and  $u(\mathbf{y}, t)$  has a temporal period  $\tilde{L}_t = \kappa L_t / L_y^2$ . It is convenient to introduce two different scales in time:  $t$  (slow),  $\tau = t/\epsilon^2$  (fast). Consequently, the differential operators in time will be replaced  $\partial_t \rightarrow \partial_t + \frac{1}{\epsilon^2} \partial_\tau$  and the equation becomes

$$\partial_t c_i + \frac{1}{\epsilon^2} \partial_\tau c_i + \frac{\text{Pe}}{\epsilon} u(\mathbf{y}, \tau) \partial_x c_i = \kappa_i \partial_x (\partial_x c_i + z_i c_i \partial_x \phi) + \frac{\kappa_i}{\epsilon^2} \nabla_{\mathbf{y}} \cdot (\nabla_{\mathbf{y}} c_i + z_i c_i \nabla_{\mathbf{y}} \phi). \quad (3.3)$$

Notice that the equation is invariant under the translation in  $x$ . For convenience, one can consider applying the Galilean transformation  $\tilde{x} = x - \langle u(\mathbf{y}, \tau) \rangle_{\mathbf{y}, \tau} t$  so that the

resulting new shear flow  $\tilde{u} = u - \langle u(\mathbf{y}, \tau) \rangle_{\mathbf{y}, \tau}$  has a zero average, where the average of a function is defined as  $\langle f(\mathbf{y}, \tau) \rangle_{\mathbf{y}, t} = \frac{1}{|\Omega|\tilde{L}_t} \int_{\Omega} \int_0^{\tilde{L}_t} f(\mathbf{y}, \tau) d\mathbf{y} d\tau$ .

Assuming the asymptotic expansion of  $c_i$  in the limit  $\epsilon \rightarrow 0$  is

$$c_i(x, \mathbf{y}, t) = c_{i,0}(x, y, t, \tau) + \epsilon c_{i,1}(x, y, t, \tau) + \epsilon^2 c_{i,2}(x, y, t, \tau) + \mathcal{O}(\epsilon^3). \quad (3.4)$$

Substituting the asymptotic expansion of  $c_i$  into the formula for  $\phi$  and using the Taylor expansion yield the asymptotic expansion of  $\phi$ , i.e.,  $\phi = \phi_0 + \epsilon \phi_1 + \epsilon^2 \phi_2 + \mathcal{O}(\epsilon^3)$ . In particular, the gradient of the first two coefficients are given by

$$\begin{aligned} \nabla \phi_0 &= \frac{\sum_{i=1}^{n-1} (\kappa_n - \kappa_i) z_i \nabla c_{i,0}}{\sum_{i=1}^{n-1} (z_i \kappa_i - z_n \kappa_n) z_i c_{i,0}}, \\ \nabla \phi_1 &= \frac{\sum_{i=1}^{n-1} (\kappa_n - \kappa_i) z_i \nabla c_{i,1}}{\sum_{i=1}^{n-1} (z_i \kappa_i - z_n \kappa_n) z_i c_{i,0}} + \frac{\left( \sum_{i=1}^{n-1} (\kappa_n - \kappa_i) z_i \nabla c_{i,0} \right) \left( \sum_{i=1}^{n-1} (z_i \kappa_i - z_n \kappa_n) z_i c_{i,1} \right)}{\left( \sum_{i=1}^{n-1} (z_i \kappa_i - z_n \kappa_n) z_i c_{i,0} \right)^2}. \end{aligned} \quad (3.5)$$

Substituting the expansion of  $c_i$  and  $\nabla \phi$  into equation (3.3) leads to an equation involving the power series of  $\epsilon$ . Since the equation holds for arbitrarily small  $\epsilon$ , the coefficient of each power of  $\epsilon$  should be zero, which yields a hierarchy of equations of  $c_{i,k}$ .

Grouping all term of order  $\mathcal{O}(\epsilon^{-2})$  and setting the coefficient to be zero yield the equation

$$\partial_\tau c_{i,0} = \kappa_i \nabla_{\mathbf{y}} \cdot (\nabla_{\mathbf{y}} c_{i,0} + z_i c_{i,0} \nabla_{\mathbf{y}} \phi_0), \quad c_{i,0}|_{t=0, \tau=0} = c_{I,i}(x). \quad (3.6)$$

The initial condition is a function of the variable  $x$  only, which means that  $c_{i,0}(x, \mathbf{y}, t, \tau) = c_{i,0}(x, t)$ ,  $i = 1, \dots, n$ . Consequently, the evolution equation for  $c_{i,0}$  provides the desired approximation. The goal of this homogenization calculation is to derive this equation.

Grouping all term of order  $\mathcal{O}(\epsilon^{-1})$  yields the equation

$$\partial_\tau c_{i,1} + \text{Pe} u(\mathbf{y}, \tau) \partial_x c_{i,0} = \kappa_i \nabla_{\mathbf{y}} \cdot (\nabla_{\mathbf{y}} c_{i,1} + z_i c_{i,1} \nabla_{\mathbf{y}} \phi_0 + z_i c_{i,0} \nabla_{\mathbf{y}} \phi_1), \quad (3.7)$$

with the initial condition  $c_{i,1}|_{t=0, \tau=0} = 0$  and the no-flux boundary condition  $\mathbf{n} \cdot \nabla c_{i,1}|_{\mathbb{R} \times \partial \Omega} = 0, i = 1, \dots, n-1$ . Since  $c_{i,0}$  is independent of  $\mathbf{y}$ , equation (3.5) implies

$$\nabla_{\mathbf{y}} \phi_0 = 0, \quad \nabla_{\mathbf{y}} \phi_1 = \frac{\sum_{i=1}^{n-1} (\kappa_n - \kappa_i) z_i \nabla_{\mathbf{y}} c_{i,1}}{\sum_{i=1}^{n-1} (z_i \kappa_i - z_n \kappa_n) z_i c_{i,0}}. \quad (3.8)$$

Therefore, equation (3.7) is a linear equation of  $c_{i,1}$ ,

$$\begin{aligned} \partial_\tau \mathbf{c}_1 + \text{Pe} u(\mathbf{y}, \tau) \partial_x \mathbf{c}_0 &= \mathbf{D}(\mathbf{c}_0) \Delta_{\mathbf{y}} \mathbf{c}_1, \\ \mathbf{D} &= \begin{bmatrix} \kappa_1 & \dots & 0 \\ & \dots & \\ 0 & \dots & \kappa_{n-1} \end{bmatrix} - \begin{bmatrix} \kappa_1 z_1 c_{1,0} & & \\ & \dots & \\ \kappa_{n-1} z_{n-1} c_{n-1,0} & & \end{bmatrix} \frac{[(\kappa_1 - \kappa_n) z_1, \dots, (\kappa_{n-1} - \kappa_n) z_{n-1}]}{\sum_{i=1}^{n-1} (z_i \kappa_i - z_n \kappa_n) z_i c_{i,0}}, \end{aligned} \quad (3.9)$$

where  $\mathbf{c}_0 = (c_{1,0}, \dots, c_{n-1,0})$ ,  $\mathbf{c}_1 = (c_{1,1}, \dots, c_{n-1,1})$ ,  $\Delta_{\mathbf{y}} = \sum_{i=1}^d \partial_{y_i}^2$ , and  $\Delta_{\mathbf{y}} \mathbf{c}_1 = (\Delta_{\mathbf{y}} c_{1,1}, \dots, \Delta_{\mathbf{y}} c_{n-1,1})$ . For unsteady shear flow  $u(\mathbf{y}, t)$ , the solution of this diffusion equation can be expressed as

$$\mathbf{c}_1 = \text{Pe}(-\partial_\tau + \mathbf{D}\Delta_{\mathbf{y}})^{-1} (u \partial_x \mathbf{c}_0). \quad (3.10)$$

For the steady shear flow  $u(\mathbf{y})$ , the expression simplifies to

$$\mathbf{c}_1 = \text{Pe} \Delta_{\mathbf{y}}^{-1} (u) \mathbf{D}^{-1} \partial_x \mathbf{c}_0, \quad (3.11)$$

where the inverse of  $\mathbf{D}$  is available from the Sherman–Morrison formula (see Sherman & Morrison (1950))

$$\mathbf{D}^{-1} = \begin{bmatrix} \frac{1}{\kappa_1} & \cdots & 0 \\ & \ddots & \\ 0 & \cdots & \frac{1}{\kappa_{n-1}} \end{bmatrix} \left( I + \begin{bmatrix} \kappa_1 z_1 c_{1,0} \\ \vdots \\ \kappa_{n-1} z_{n-1} c_{n-1,0} \end{bmatrix} \frac{\left[ \frac{(\kappa_1 - \kappa_n) z_1}{\kappa_1}, \dots, \frac{(\kappa_{n-1} - \kappa_n) z_{n-1}}{\kappa_{n-1}} \right]}{\kappa_n \sum_{i=1}^{n-1} (z_i - z_n) z_i c_{i,0}} \right), \quad (3.12)$$

where  $I$  is the identity matrix. Moreover, one can obtain  $\mathbf{D}^{-1}$  by replacing  $\kappa_i$  and  $c_i$  with  $\kappa_i^{-1}$  and  $c_i \kappa_i$  respectively in  $\mathbf{D}$ , namely,

$$\mathbf{D}^{-1}(c_1, \dots, c_{n-1}, \kappa_1, \dots, \kappa_{n-1}) = \mathbf{D}(c_1 \kappa_1, \dots, c_{n-1} \kappa_{n-1}, \kappa_1^{-1}, \dots, \kappa_{n-1}^{-1}), \quad (3.13)$$

which suggests that  $\mathbf{D}^{-1}$  is the diffusion tensor for a system with different diffusivities and concentrations.

Additionally concern is that whether equation (3.9) is solvable. Fredholm solvability states that the linear equation  $\mathcal{L}\Psi = f$  has a solution if and only if  $\langle fg \rangle = 0$  for any solution of equation  $\mathcal{L}^*g = 0$ , where  $\mathcal{L}^*$  is the adjoint operator of  $\mathcal{L}$ . Here, the constant function solves the adjoint problem and the solvability condition of (3.9) is guaranteed by the assumption that the average of flow is zero

$$\langle \text{Pe} u(\mathbf{y}, \tau) \partial_x \mathbf{c}_0 \rangle_{\mathbf{y}, \tau} = \text{Pe} \langle u(\mathbf{y}, \tau) \rangle_{\mathbf{y}, \tau} \partial_x \mathbf{c}_0 = 0. \quad (3.14)$$

Grouping all  $\mathcal{O}(\epsilon^0)$  terms yields the equation

$$\begin{aligned} & \partial_t c_{i,0} + \partial_\tau c_{i,2} + \text{Pe} u(\mathbf{y}, \tau) \partial_x c_{i,1} \\ &= \kappa_i \partial_x (\partial_x c_{i,0} + z_i c_{i,0} \partial_x \phi_0) + \kappa_i \nabla_{\mathbf{y}} \cdot (\nabla_{\mathbf{y}} c_{i,2} + z_i (c_{i,2} \nabla_{\mathbf{y}} \phi_0 + 2c_{i,1} \nabla_{\mathbf{y}} \phi_1 + c_{i,0} \nabla_{\mathbf{y}} \phi_2)). \end{aligned} \quad (3.15)$$

In order to ensure the existence of a solution, the solvability condition requires the forcing term to have a zero average. When no-flux boundary conditions are imposed and the divergence theorem is applied, the average of the last term on the right-hand side of the above equation is shown to be zero. Therefore, the solvability condition can be expressed as

$$\partial_t c_{i,0} + \text{Pe} \langle u(\mathbf{y}, \tau) \partial_x c_{i,1} \rangle_{\mathbf{y}, \tau} = \kappa_i \partial_x (\partial_x c_{i,0} + z_i c_{i,0} \partial_x \phi_0). \quad (3.16)$$

One can eliminate  $c_{i,1}$  using equation (3.10) and obtain the equation of  $c_{i,0}$

$$\partial_t \mathbf{c}_0 + \text{Pe}^2 \partial_x \langle u(\mathbf{D}\Delta_{\mathbf{y}} - \partial_\tau)^{-1} (u \partial_x \mathbf{c}_0) \rangle_{\mathbf{y}, \tau} = \partial_x (\mathbf{D} \partial_x \mathbf{c}_0), \quad (3.17)$$

where  $\mathbf{D}$  is defined in equation (3.9). For the steady shear flow, the equation reduces to

$$\partial_t \mathbf{c}_0 + \text{Pe}^2 \partial_x \langle u \Delta_{\mathbf{y}}^{-1} u \rangle_{\mathbf{y}, \tau} \mathbf{D}^{-1} \partial_x \mathbf{c}_0 = \partial_x (\mathbf{D} \partial_x \mathbf{c}_0). \quad (3.18)$$

The explicit expression of the coefficient  $\langle u \Delta_{\mathbf{y}}^{-1} u \rangle_{\mathbf{y}, \tau}$  for some classical flows and the flow used in the numerical simulation can be found in appendix A.

The constant coefficient nonlinear equations (3.18) is an approximation of equation (2.1) in the limit of  $\epsilon \rightarrow 0$ , as well as at long times. It is worth noting that, as time elapses, the diffusion term in equation (2.1) smooths out the solution, which leads to an increase in the length scale of the solution and a decrease in the ratio  $\epsilon = \frac{L_y}{L_x}$ .

### 3.2. Self-similar solution of the effective equation

Deriving the exact solution of the initial value problem (3.17) and (3.18) is challenging. However, investigating the long-term behavior of the reaction-diffusion equation is possible, as it typically converges to its similarity solution (Gupta *et al.* (2019); Wang & Roberts (2013); Barenblatt & Isaakovich (1996); Eggers & Fontelos (2008)). For the first type of initial condition, where the solution vanishes at infinity, such as the classical diffusion equation, the scaling relation of equations (3.17) and (3.18) allows for a self-similar solution of the following form

$$c_{i,0}(x, t) = \frac{1}{\sqrt{t}} C_i(\xi), \quad \xi = \frac{x}{\sqrt{t}}. \quad (3.19)$$

The conservation of mass imposes an additional condition  $\int_{-\infty}^{\infty} C_i(\xi) d\xi = \int_{-\infty}^{\infty} c_{I,i}(x) dx$ . In fact, with the change of variable  $\tau = \log t$ ,  $\xi = t^{-\frac{1}{2}}x$  and  $\mathbf{c}(x, t) = t^{-\frac{1}{2}}\mathbf{C}(\xi, \tau)$ , equation (3.18) becomes

$$\partial_\tau \mathbf{C} = \frac{1}{2} \mathbf{C} + \frac{\xi}{2} \partial_\xi \mathbf{C} - \text{Pe}^2 \partial_\xi \langle u \Delta_{\mathbf{y}}^{-1} u \rangle_{\mathbf{y}, \tau} \mathbf{D}^{-1} \partial_\xi \mathbf{C} + \partial_\xi \mathbf{D}(\mathbf{C}) \partial_\xi \mathbf{C}, \quad (3.20)$$

where  $\mathbf{C} = (C_1, \dots, C_{n-1})$ . The self-similarity solution is the steady solution of this equation, which satisfies

$$0 = \frac{1}{2} \mathbf{C} + \frac{\xi}{2} \partial_\xi \mathbf{C} - \text{Pe}^2 \partial_\xi \langle u \Delta_{\mathbf{y}}^{-1} u \rangle_{\mathbf{y}, \tau} \mathbf{D}^{-1} \partial_\xi \mathbf{C} + \partial_\xi \mathbf{D}(\mathbf{C}) \partial_\xi \mathbf{C}. \quad (3.21)$$

Integrating both side of the equation and using the vanishing condition at infinity reduces the equation to

$$0 = \frac{\xi}{2} \mathbf{C} - \text{Pe}^2 \langle u \Delta_{\mathbf{y}}^{-1} u \rangle_{\mathbf{y}, \tau} \mathbf{D}^{-1} \partial_\xi \mathbf{C} + \mathbf{D}(\mathbf{C}) \partial_\xi \mathbf{C}. \quad (3.22)$$

While the self-similarity solution of the ion concentration may not be a Gaussian distribution function, it has the property

$$\int_{-\infty}^{\infty} x^n c_{i,0}(x, t) dx = \int_{-\infty}^{\infty} \frac{x^n}{\sqrt{t}} C_i\left(\frac{x}{\sqrt{t}}\right) dx = t^{\frac{n}{2}} \int_{-\infty}^{\infty} \xi^n C_i(\xi) d\xi. \quad (3.23)$$

This equation implies that the second moment of the ion concentration,  $\frac{1}{|\Omega|} \int_{-\infty}^{\infty} x^2 c_i(x, \mathbf{y}, t) d\mathbf{y} dx$ , grows linearly asymptotically for large  $t$ . Since  $\bar{c}_i$  converges to  $c_{i,0}$  at long times, the longitudinal effective diffusivity of  $i$ -th ion defined in equation (2.4) can be expressed in terms of  $C_i$

$$\kappa_{\text{eff},i} = \lim_{t \rightarrow \infty} \frac{\int_{-\infty}^{\infty} x^2 c_{i,0}(x, t) dx - \left( \int_{-\infty}^{\infty} x c_{i,0}(x, t) dx \right)^2}{2t \int_{-\infty}^{\infty} c_{i,0} dx} = \frac{\int_{-\infty}^{\infty} \xi^2 C_i(\xi) d\xi - \left( \int_{-\infty}^{\infty} \xi C_i(\xi) d\xi \right)^2}{2 \int_{-\infty}^{\infty} C_i(\xi) d\xi}. \quad (3.24)$$

The previous definition (2.4) required advancing the solution of the governing equation in the full domain (a high-dimensional space) until the diffusion time scale was resolved. In contrast, the definition (3.24) present here only requires solving the steady-state solution of the effective equation that depends on one variable, which is more computationally efficient.

For the second type of initial condition, where the background ion concentration is nonzero, one can search for the asymptotic expansion of the concentration field in the following form

$$c_{i,0}(x, t) = c_i(\infty) + \frac{1}{\sqrt{t}} C_i(\xi) + o\left(t^{-\frac{1}{2}}\right). \quad (3.25)$$

Substituting this expression into equation (3.18) and taking the limit  $t \rightarrow \infty$  yields the equation for  $C_i$

$$0 = \frac{1}{2} \mathbf{C} + \frac{\xi}{2} \partial_\xi \mathbf{C} + \partial_\xi \left( \tilde{\mathbf{D}} - \text{Pe}^2 \langle u \Delta_{\mathbf{y}}^{-1} u \rangle_{\mathbf{y}, \tau} \tilde{\mathbf{D}}^{-1} \right) \partial_\xi \mathbf{C}. \quad (3.26)$$

where  $\tilde{\mathbf{D}}$  and  $\tilde{\mathbf{D}}^{-1}$  are constant matrices

$$\begin{aligned} \mathbf{D} &= \begin{bmatrix} \kappa_1 & \dots & 0 \\ & \dots & \\ 0 & \dots & \kappa_{n-1} \end{bmatrix} - \begin{bmatrix} \kappa_1 z_1 c_1(\infty) & & \\ & \dots & \\ \kappa_{n-1} z_{n-1} c_{n-1}(\infty) & & \end{bmatrix} \frac{[(\kappa_1 - \kappa_n) z_1, \dots, (\kappa_{n-1} - \kappa_n) z_{n-1}]}{\sum_{i=1}^{n-1} (z_i \kappa_i - z_n \kappa_n) z_i c_i(\infty)}, \\ \tilde{\mathbf{D}}^{-1} &= \begin{bmatrix} \frac{1}{\kappa_1} & \dots & 0 \\ & \dots & \\ 0 & \dots & \frac{1}{\kappa_{n-1}} \end{bmatrix} \left( I + \begin{bmatrix} \kappa_1 z_1 c_1(\infty) & & \\ & \dots & \\ \kappa_{n-1} z_{n-1} c_{n-1}(\infty) & & \end{bmatrix} \frac{\left[ \frac{(\kappa_1 - \kappa_n) z_1}{\kappa_1}, \dots, \frac{(\kappa_{n-1} - \kappa_n) z_{n-1}}{\kappa_{n-1}} \right]}{\kappa_n \sum_{i=1}^{n-1} (z_i - z_n) z_i c_i(\infty)} \right). \end{aligned} \quad (3.27)$$

The constant diffusion tensor implies that for a non-zero background ion concentration, the perturbed concentrations satisfy a multi-dimensional diffusion equation at long times. The expression of the diffusion tensor provides a formula for measuring the mutual diffusion coefficients. It is worth noting that if the background ion concentration is smaller compared to the perturbed concentration, the system will take a longer time to reach this long-time asymptotic state.

For the third type of initial condition, the self-similar solution takes the form

$$c_{i,0}(x, t) = C_i(\xi), \quad \xi = \frac{x}{\sqrt{t}}, \quad (3.28)$$

where  $C_i(\xi)$  solves

$$0 = \frac{\xi}{2} \partial_\xi \mathbf{C} - \text{Pe}^2 \partial_\xi \langle u \Delta_{\mathbf{y}}^{-1} u \rangle_{\mathbf{y}, \tau} \mathbf{D}^{-1} \partial_\xi \mathbf{C} + \partial_\xi \mathbf{D}(\mathbf{C}) \partial_\xi \mathbf{C}. \quad (3.29)$$

It is easy to show that the second moment of the derivative of the solution grows linearly in  $t$ ,

$$\frac{1}{|\Omega|} \int_{-\infty}^{\infty} x^2 \partial_x c_{i,0}(x, \mathbf{y}, t) d\mathbf{y} dx \approx \int_{-\infty}^{\infty} \frac{x^2}{\sqrt{t}} \partial_\xi C_i \left( \frac{x}{\sqrt{t}} \right) dx = t \int_{-\infty}^{\infty} \xi^2 \partial_\xi C_i(\xi) d\xi. \quad (3.30)$$

Therefore, we can also define the effective diffusivity via the self-similarity solution,

$$\kappa_{\text{eff},i} = \frac{\int_{-\infty}^{\infty} \xi^2 \partial_{\xi} C_i(\xi) d\xi - \left( \int_{-\infty}^{\infty} \xi \partial_{\xi} C_i(\xi) d\xi \right)^2}{2 \int_{-\infty}^{\infty} \partial_{\xi} C_i(\xi) d\xi}. \quad (3.31)$$

When the diffusion tensor is constant such as the case that diffusion-induced electric potential is negligible, the first and third types of initial conditions result in the same effective diffusivity, as the equation of the self-similarity solution commute with the differential operator. However, if the diffusion tensor varies with concentration, these two types of initial conditions can yield different effective diffusivities. Nonetheless, in the examples presented in the following sections, the relative difference is less than 0.03.

### 3.3. Comparison to the Taylor dispersion

When the diffusion-induced electric potential is negligible, the governing equation becomes the advection-diffusion equation

$$\partial_t c_i + u(\mathbf{y}, t) \partial_x c_i = \kappa_i \Delta c_i, \quad i = 1, \dots, n. \quad (3.32)$$

The corresponding effective equation has been reported in many literature of Taylor dispersion (Taylor (2012); Ding *et al.* (2021); Young & Jones (1991))

$$\partial_t c_{i,0} = \kappa_{\text{eff},i} \partial_x^2 c_{i,0}, \quad \kappa_i + \frac{\text{Pe}^2}{\kappa_i} \langle u(\partial_{\tau} - \Delta)^{-1} u \rangle_{\mathbf{y},\tau}, \quad i = 1, \dots, n. \quad (3.33)$$

Therefore, equation (3.18) can be considered to be a generalization of equation (3.33) with a nonlinear diffusion tensor taking the place of a scalar diffusion coefficient. Additionally, both equations exhibit a “reciprocal property” whereby, under strong shear flow, the system behaves as if it were a different system with distinct parameters and no flow.

For large Péclet numbers,  $\kappa_{\text{eff},i} \approx \frac{\text{Pe}^2}{\kappa_i} \langle u(\partial_{\tau} - \Delta)^{-1} u \rangle_{\mathbf{y},\tau}$  in equation (3.33). After rescaling  $\text{Pe} \tilde{x} \sqrt{\langle u(\partial_{\tau} - \Delta)^{-1} u \rangle_{\mathbf{y},\tau}} = x$ , equation (3.33) becomes a diffusion equation with the diffusion coefficient  $\frac{1}{\kappa_i}$ . Similarly, for large Péclet numbers, equation (3.18) can be approximated by

$$\partial_t \mathbf{c}_0 + \text{Pe}^2 \partial_x \langle u \Delta_{\mathbf{y}}^{-1} u \rangle_{\mathbf{y},\tau} \mathbf{D}^{-1} \partial_x \mathbf{c}_0 = 0. \quad (3.34)$$

The relation between the diffusion tensor  $\mathbf{D}$  and its inverse  $\mathbf{D}^{-1}$  provided in equation (3.13) ensures that the effective equation (3.17) has the same property. After rescaling using  $\text{Pe} \tilde{x} \sqrt{\langle u(-\Delta)^{-1} u \rangle_{\mathbf{y},\tau}} = x$ , the equation can be written as the Nernst-Planck equation in the absence of flow, with diffusivities  $\kappa_1^{-1}, \dots, \kappa_{n-1}^{-1}$  and concentrations  $c_1 \kappa_1, \dots, c_{n-1} \kappa_{n-1}$ :

$$\partial_t \mathbf{c}_0 = \partial_{\tilde{x}} \left( \mathbf{D} \left( c_1 \kappa_1, \dots, c_{n-1} \kappa_{n-1}, \kappa_1^{-1}, \dots, \kappa_{n-1}^{-1} \right) \partial_{\tilde{x}} \mathbf{c}_0 \right). \quad (3.35)$$

The reciprocal property observed in the effective equations has two implications. First, for strong flows, it simplifies the problem to the Nernst-Planck equation in the absence of flow. Second, it establishes a correspondence between phenomena observed in systems with and without flow, allowing us to expect similar behavior in different systems.

## 4. Examples and numerical tests

In this section, a series of examples will be analyzed to gain a deeper understanding of how individual ion diffusivities interact and impact the overall dynamics of dissolved salt.

### 4.1. Two different ion species

We first consider the simplest example where the solution consists of two different type of ion species. When  $n = 2$ , the diffusion tensor provided in equation (3.9) and its inverse matrix are scalars. Effective equation (3.18) becomes a diffusion equation

$$\partial_t c_{1,0} = \kappa_{\text{eff},1} \partial_x^2 c_{1,0}, \quad \kappa_{\text{eff},1} = \left( \frac{\kappa_1 \kappa_2 (z_1 - z_2)}{\kappa_1 z_1 - \kappa_2 z_2} - \text{Pe}^2 \langle u \Delta_{\mathbf{y}}^{-1} u \rangle_{\mathbf{y},\tau} \frac{\kappa_1 z_1 - \kappa_2 z_2}{\kappa_1 \kappa_2 (z_1 - z_2)} \right). \quad (4.1)$$

Deen (1998) shows that, in absence of flow, the Nernst-Planck equation reduces to a diffusion equation with a constant diffusion coefficient  $\frac{\kappa_1 \kappa_2 (z_1 - z_2)}{\kappa_1 z_1 - \kappa_2 z_2}$ . The calculation here verifies that this result also holds in presence of the shear flow. Therefore, the transport of binary electrolyte solution can be described by the classical Taylor dispersion theory.

### 4.2. Three different ion species

Many physical systems contains three different ion species, such as the ternary electrolyte solutions and the mixture of two the binary electrolyte solutions, e.g, the mixture of sodium fluorescein and sodium chloride. When  $n = 3$ , the diffusion tensor provided in equation (3.9) and its inverse matrix depend on the ion concentrations, in contrast to the case with  $n = 2$ ,

$$\mathbf{D} = \begin{bmatrix} \kappa_1 - \frac{c_1 \kappa_1 (\kappa_1 - \kappa_3) z_1^2}{c_1 z_1 (\kappa_1 z_1 - \kappa_3 z_3) + c_2 z_2 (\kappa_2 z_2 - \kappa_3 z_3)} & - \frac{c_1 \kappa_1 (\kappa_2 - \kappa_3) z_1 z_2}{c_1 z_1 (\kappa_1 z_1 - \kappa_3 z_3) + c_2 z_2 (\kappa_2 z_2 - \kappa_3 z_3)} \\ - \frac{c_2 \kappa_2 (\kappa_1 - \kappa_3) z_1 z_2}{c_1 z_1 (\kappa_1 z_1 - \kappa_3 z_3) + c_2 z_2 (\kappa_2 z_2 - \kappa_3 z_3)} & \kappa_2 - \frac{c_2 \kappa_2 (\kappa_2 - \kappa_3) z_2^2}{c_1 z_1 (\kappa_1 z_1 - \kappa_3 z_3) + c_2 z_2 (\kappa_2 z_2 - \kappa_3 z_3)} \end{bmatrix}, \quad (4.2)$$

$$\mathbf{D}^{-1} = \begin{bmatrix} \frac{c_2 \kappa_3 z_2 (z_2 - z_3) + c_1 z_1 (\kappa_1 z_1 - \kappa_3 z_3)}{\kappa_1 \kappa_3 (c_1 z_1 (z_1 - z_3) + c_2 z_2 (z_2 - z_3))} & \frac{c_1 (\kappa_2 - \kappa_3) z_1 z_2}{\kappa_2 \kappa_3 (c_1 z_1 (z_1 - z_3) + c_2 z_2 (z_2 - z_3))} \\ \frac{c_2 (\kappa_1 - \kappa_3) z_1 z_2}{\kappa_1 \kappa_3 (c_1 z_1 (z_1 - z_3) + c_2 z_2 (z_2 - z_3))} & \frac{c_1 \kappa_3 z_1 (z_1 - z_3) + c_2 z_2 (\kappa_2 z_2 - \kappa_3 z_3)}{\kappa_2 \kappa_3 (c_1 z_1 (z_1 - z_3) + c_2 z_2 (z_2 - z_3))} \end{bmatrix}.$$

As a result, the effective equation (3.18) remains nonlinear, which leads to many interesting phenomena which can't be observed in the binary electrolyte solution. We will illustrate that via the simulation the following example.

The simulation uses the Fourier spectral method described in (Ding & McLaughlin (2022)). The computational domain is  $(x, y) \in [-8\pi, 8\pi] \times [0, 1]$ . The shear flow is  $u(y) = \text{Pecos} 2\pi y$  and the corresponding effective equation is provided in equation (A 4). We choose this flow for two reasons. First, it can be fully resolved in the Fourier spectral algorithm and ensure higher accuracy. Second, the flow profile is close to the pressure-driven flow. When the background concentration is nonzero, the system can be described by the Taylor dispersion theory. In this section, the initial conditions are assumed to be of the following form unless stated otherwise,  $c_{I,1} = c_{I,2} = \frac{1}{\sigma\sqrt{2\pi}} e^{-\frac{1}{2}(\frac{x}{\sigma})^2}$ , where

$\sigma = \frac{1}{4}$ . In this case,  $\int_{-\infty}^{\infty} \int_0^1 c_{I,1} dy dx = \int_{-\infty}^{\infty} \int_0^1 c_{I,2} dy dx = 1$ . The diffusivities and valence are  $\kappa_1 = 1, \kappa_2 = 0.1, \kappa_3 = 1, z_1 = 1, z_2 = 1, z_3 = -2$ .

#### 4.2.1. Transverse variations

The concentration fields in the channel undergo a transition from an initially inhomogeneous distribution to a homogenized distribution over long timescales. To study

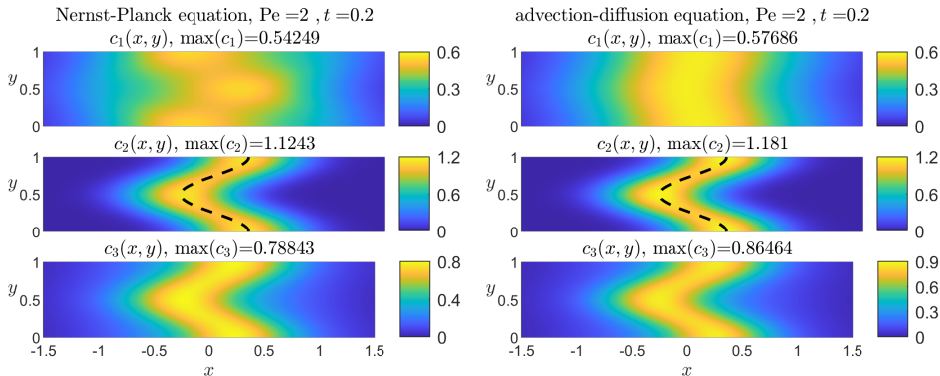


FIGURE 2. Numerical solution to equation (2.3) (left panel) and (3.32) (right panel) at  $t = 0.2$ . The parameters are  $\kappa_1 = 1, \kappa_2 = 0.1, \kappa_3 = 1, z_1 = 1, z_2 = 1, z_3 = -2, \text{Pe} = 2$ . The black dashed lines depict the shape of the shear flow profile.

the dynamics of this transition, we begin by performing numerical simulations of the governing equation (2.3), which reveal that the system undergoes complex behavior as it approaches the homogenized state.

The left panel of figure 2 shows the solution of equation (2.3) at an early stage,  $t = 0.2$ . For comparison, the right panel of Figure 2 presents the result when the electric potential is negligible, i.e., the solution of the advection-diffusion equation (3.32). When the simulation time is small compared to the diffusion timescale, the shear flow advection dominates, and one would expect the concentration field to follow the shear flow profile, as shown in the right column of figure 2. In the left column, the concentration fields of the second and third ion species also follow the shear flow profile. However, for the first ion species, the concentration field does not follow the expected behavior and instead bends in the opposite direction to the shear flow, as shown in the middle-left plot of Figure 2. This behavior is the result of the electric interaction between ions. Both the first and second ion species are cations, so the repulsive electromagnetic force pushes ions away from each other. If one of them follows the shear flow profile, the other one will bend in the opposite direction. As a result, the second ion species visually migrates upstream.

It is interesting to see how concentration distribution changes at larger time scales where diffusion has a greater influence. The left panel of figure 3 presents the numerical solution for equation (2.3) at a larger time  $t = 2$ . As expected, all concentration profiles are more blurred due to diffusion. The concentration profiles of the first and second ions still bend in opposite directions. On the right panel, we compare the cross-sectional averaged concentration field with the solution to the effective equation (A 4) that was derived using the homogenization method. The curves perfectly overlap, demonstrating the validity of the homogenization calculation. It's worth noting that due to the assumption of the asymptotic analysis, the effective equation is valid for small  $\epsilon$  or large  $t$ , where  $\epsilon = \frac{L_y}{L_x}$  and  $L_x$  and  $L_y$  are characteristic lengths of the initial condition and the channel width, respectively. In this numerical test case, we have  $L_x = \frac{1}{4}$ ,  $L_y = 1$  and  $\epsilon = 4$ . The diffusion time scale is  $\max(\kappa_1^{-1}, \kappa_2^{-1}, \kappa_3^{-1}) = 10$ , indicating that the parameter regime for the effective equation to reach a good approximation is larger than previously thought.

The variations of the concentration field across the channel are different for a stronger flow. Figure 4 presents the numerical solutions to the advection-Nernst-Planck equation (2.3) for a stronger flow with  $\text{Pe} = 8$  at  $t = 0.2$  (left panel) and  $t = 1$  (right panel). We

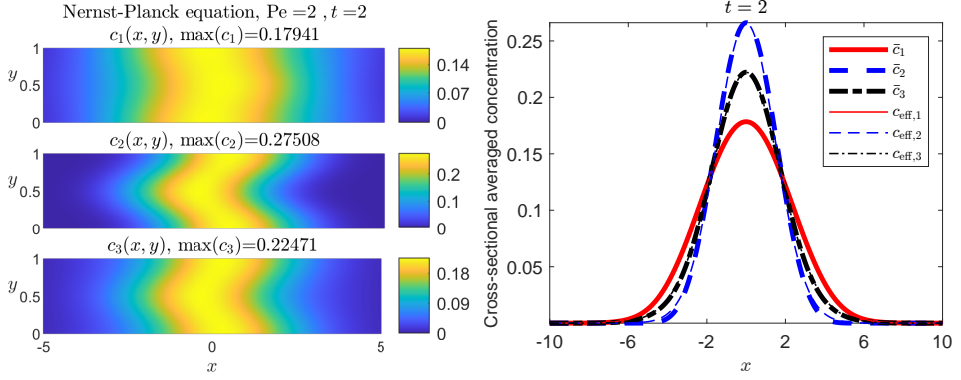


FIGURE 3. The left panel shows the numerical solution to equation (2.3) at  $t = 2$ . The parameters are  $\kappa_1 = 1, \kappa_2 = 0.1, \kappa_3 = 1, z_1 = 1, z_2 = 1, z_3 = -2, \text{Pe} = 2$ . In the right panel, the thicker curves represent the cross-sectional average of concentration fields presented in the left panel,  $\bar{c}(x, t) = \frac{1}{|\Omega|} \int_{\Omega} c(x, \mathbf{y}, t) d\mathbf{y}$ . The thinner curve represents the solution of effective equation (A 4).

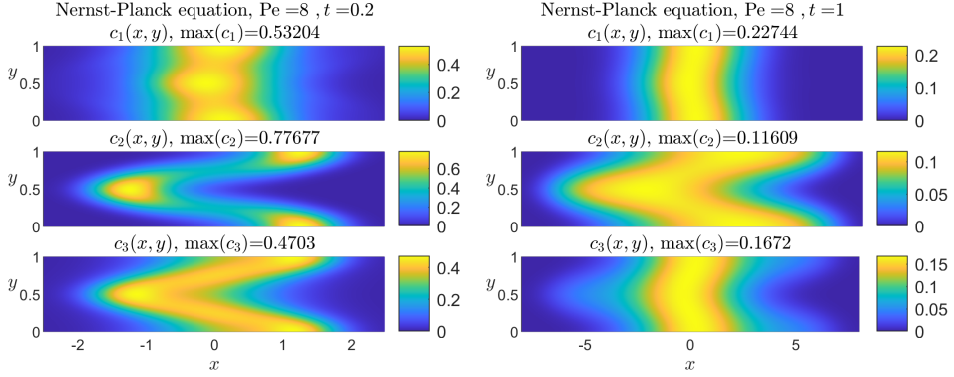


FIGURE 4. The numerical solution to equation (2.3) with  $\text{Pe} = 8$  at  $t = 0.2$  (left panel),  $t = 1$  (right panel). The parameters are  $\kappa_1 = 1, \kappa_2 = 0.1, \kappa_3 = 1, z_1 = 1, z_2 = 1, z_3 = -2$ .

have several observations. Firstly, the effect of flow becomes more prominent over the ion-electric interaction, resulting in all concentration profiles bending in the direction of the shear flow. This is in contrast to the case of weak flow, where the concentration profiles of the first and second ion species bend in opposite directions due to the ion-electric interaction. Secondly, at the early stages, there is a clearer separation between the first and second ion species, with the majority of the first ion species remaining near their original positions, while the second ion species are pushed away by the electromagnetic force. However, due to diffusion, the solutions homogenize and the separation becomes weaker as time increases. This homogenization is evident in the right panel of figure 4, where the separation is no longer visible. The third observation is that the different ion species have different spreading rates in the longitudinal direction. The second ion species, with the smallest diffusivity, spreads the most. These unexpected results highlight the importance of studying effective diffusivity in understanding the transport of ions in microchannels under flow conditions.

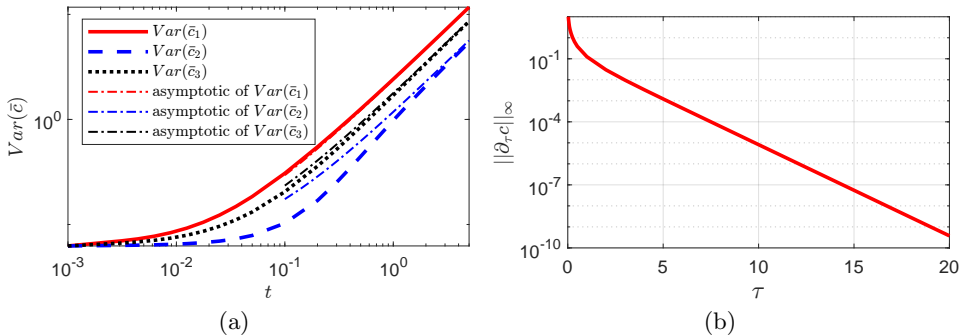


FIGURE 5. (a) Comparison between the variance of the numerical solutions for (2.3) (thicker curves) and their theoretical asymptotics (thinner curves) log-log scale. The numerical solutions at  $t = 2$  are plotted in figure 3. The asymptotics of the variance is provided in equation (2.5). In this case,  $Var(\bar{c}_i) \approx 2t\kappa_{\text{eff},i} + \sigma^2$ , where  $\sigma = \frac{1}{4}$  and  $\kappa_{\text{eff},i}$  is defined in equation (3.24). (b) The infinity norm of  $\partial_\tau \mathbf{C}$  as a function of  $\tau$ .  $\mathbf{C}$  solves equation (3.20).

#### 4.2.2. Dependence of the effective diffusivity on Péclet numbers

In this subsection, we will further explore the dependence of the variance of the cross-sectional-averaged concentration and the effective diffusivity on the Péclet numbers. Panel (a) of figure 5 compares the variance of the longitudinal distribution of the numerical solution with the theoretical variance asymptotics for the parameter  $\kappa_1 = 1, \kappa_2 = 0.1, \kappa_3 = 1, z_1 = 1, z_2 = 1, z_3 = -2, \text{Pe} = 2$ . At a larger time scale, the variance grows linearly, and converges to the asymptotics expansions, demonstrating the validity of the asymptotic analysis.

To calculate the effective diffusivities defined in equation (2.4), we approximate them using the derivative of  $Var(\bar{c}_i)$  at  $t = 5$ , resulting in  $\kappa_{\text{eff},1} = 1.1614, \kappa_{\text{eff},2} = 0.55829, \kappa_{\text{eff},3} = 0.85984$ . On the other hand, equation (3.24) allows us to calculate the effective diffusivity via the self-similarity solution. Notice that the self-similarity solution is the steady solution of equation (3.20). Therefore, we can obtain the self-similarity solution by solving the initial value problem (3.20) until the solution reaches a steady state. Panel (b) of figure 5 plots the infinity norm of  $\partial_\tau \mathbf{C}$  as a function of  $\tau$ , which verifies that the solution of the initial value problem converges to the self-similarity solution. Integrating the self-similarity solution yields  $\kappa_{\text{eff},1} = 1.1618, \kappa_{\text{eff},2} = 0.558978, \kappa_{\text{eff},3} = 0.860387$ . The effective diffusivities calculated by two different methods are consistent, demonstrating that self-similarity can accurately characterize the system's dynamics at long times. As an additional verification, we also solve the equivalent equation (3.22) for the self-similarity solution using the `NDSolve` in Mathematica, and the results are consistent up to 6 significant digits.

Figure 6 shows the effective diffusivities as a function of the Péclet number  $\text{Pe}$  for fixed parameters  $\kappa_1 = 1, \kappa_2 = 0.1, \kappa_3 = 1, z_1 = 1, z_2 = 1, z_3 = -2$ . We make three observations. First, in classical Taylor dispersion given by equation (3.33), the effective diffusivity monotonically increases with the Péclet number. In contrast, when considering the diffusion-induced electric potential, the effective diffusivities of some ion species may exhibit non-monotonic behavior with respect to the Péclet number, as shown in the inset of Figure 6. Second, the species with the largest effective diffusivity can change depending on the Péclet number. For example, the first ion species has the largest effective diffusivity for small Péclet numbers, while the second ion species has the largest effective diffusivity for large Péclet numbers, which is consistent with the observations in figures 3 and 4.

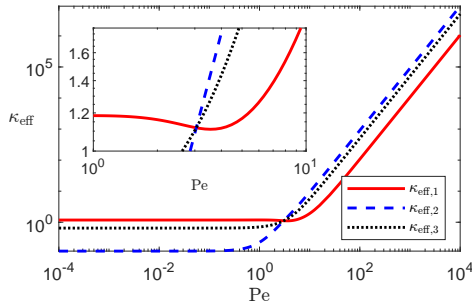


FIGURE 6. The effective diffusivities as a function of the Péclet number  $Pe$ . The inset figure show the function for the Péclet number from 1 to 10.

Finally, for large Péclet numbers, the effective diffusivity scales as  $Pe^2$ , which is the same as the classical Taylor dispersion.

Finally, it is worth noting that the effective diffusivity resulting from the initial conditions of the same type is the same. However, when the initial conditions belong to different types, even if the physical parameters and mass ratio are the same, the resulting effective diffusivity can be different. For instance, when the initial conditions are given by  $c_{I,1} = c_{I,1} = \frac{1+\text{erf}(x/2)}{2}$ , and the parameters are  $\kappa_1 = 1$ ,  $\kappa_2 = 0.1$ ,  $\kappa_3 = 1$ ,  $z_1 = 1$ ,  $z_2 = 1$ ,  $z_3 = -2$ , and  $Pe = 2$ , the effective diffusivities are  $\kappa_{\text{eff},1} = 1.1554$ ,  $\kappa_{\text{eff},2} = 0.55242$ , and  $\kappa_{\text{eff},3} = 0.85392$ . It should be noted that this result differs from the case when the initial condition is the Gaussian distribution function. While the relative difference in effective diffusivity between the initial conditions considered here is small, it is worth noting that this may not always be the case. In other parameter regimes, the difference in effective diffusivity between different initial conditions could be more significant.

#### 4.2.3. Ion separation

After the solute has been homogenized across the channel, the concentration distribution is described by a self-similar solution of the effective equation(3.21). In some parameter regimes, this self-similarity solution exhibiting properties that differ from the case without the diffusion-induced electric potential. Here, we examine the shape of this solution and explore these unique properties in more details.

The upper panel of figure 7 (a) displays the self-similarity solution  $C_i(\xi)$  for  $Pe = 0$ . Interestingly,  $C_1(\xi)$  exhibits a highly non-Gaussian shape and is not even unimodal. In the lower panel of figure 7 (a), we plot the ratio of each component  $C_i / \sum_{i=1}^3 C_i$  as a function of  $\xi$ . The ratio of the third ion species is almost constant, while the ratios of the first and second ion species vary significantly. At small values of  $\xi$ , there are more first ion species than second ion species, while at large  $\xi$ , there are virtually no first ion species in the relative sense. These results imply a spontaneous separation of ions.

By keeping the solution to the region  $|\xi| > \xi^*$  for some threshold  $\xi^*$ , which is practical for experimental implementation, we can obtain a solution that consists predominantly of the first and third ions, which implies that we can separate one binary electrolyte from the mixture of three ion species. To qualitatively investigate the ion separation, we plot the mass of each component  $M_i(\xi^*) = \int_{-\infty}^{\xi^*} C_i(\xi) d\xi + \int_{\xi^*}^{\infty} C_i(\xi) d\xi$  and their ratio  $\frac{M_2}{M_1}$  as functions of  $\xi^*$  in figure 7 panel (b). For example, by allowing a tolerance ratio of  $M_2/M_1 = 0.1$ , we can choose  $\xi^* \approx 0.9003$ , which keeps the mass  $M_1 = 0.6145$ . Note that this method can separate approximately 61% of the binary electrolytes consisting

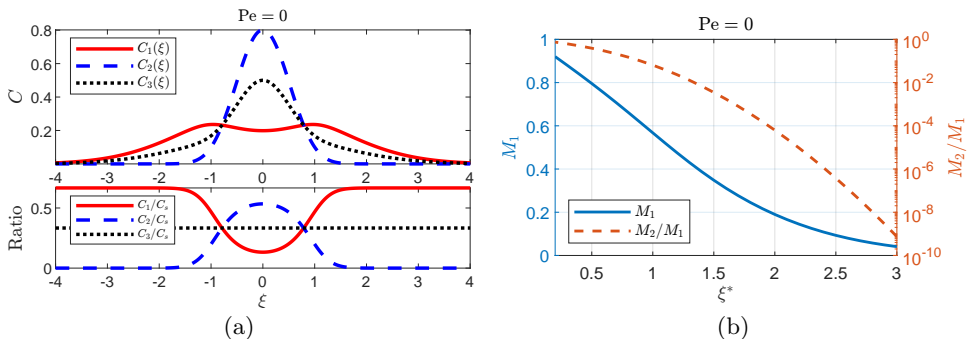


FIGURE 7. (a) The upper panel shows self-similarity solution of the effective equation with the parameters  $Pe = 0$ ,  $\kappa_1 = 1$ ,  $\kappa_2 = 0.1$ ,  $\kappa_3 = 1$ ,  $z_1 = 1$ ,  $z_2 = 1$ , and  $z_3 = -2$ . The lower panel shows the ratio of each component,  $C_i / \sum_{i=1}^3 C_i$ . (b) The blue solid curve represents  $M_1(\xi^*)$  and is associated with the left y axis. The read dashed curve represents  $M_2(\xi^*)/M_1(\xi^*)$  and is associated with the right y axis.

of the first and third ion species from the mixture of three ion species, given that the total mass of the first ion species is 1. If the tolerance ratio decreases to  $M_2/M_1 = 0.01$ , we can choose  $\xi^* \approx 1.3409$ , which still retains 41% of the first ion species.

In the presence of a shear flow, the ion separation may be weakened. Figure 8 summarizes the results for the case where the Péclet number is  $Pe = 2$ . In this case, the concentration profiles  $C_i$  become unimodal functions that are close to Gaussian distributions. Although there are still very few second ion species present in the solution for large  $\xi^*$ , the amount of first ion species that can be retained through separation is much smaller compared to the case without flow. To illustrate this, we consider a tolerance ratio of  $M_2/M_1 = 0.1$ . The optimal value of  $\xi^*$  that achieves this ratio is found to be  $\xi^* = 3.0741$ , and the mass of the separated first ion species is  $M_1 = 0.04121$ . If we reduce the tolerance ratio to  $M_2/M_1 = 0.01$ , the optimal value of  $\xi^*$  is approximately  $\xi^* \approx 4.7011$ , but the mass of the separated first ion species is much smaller, with  $M_1 = 0.001477$ . These results suggest that the separation of different ion species is weaker in the presence of a shear flow, indicating that the flow strength plays an important role in the separation process. This example suggests that the presence of a shear flow can weaken the separation of different ion species, highlighting the importance of flow strength in the separation process. However, as we discussed in section 3.3, the effective equation exhibits a reciprocal property, namely, the system without flow corresponds to the system with a strong flow and different physical parameters, which implies that the shear flow can enhance ion separation in certain parameter regimes.

#### 4.2.4. limiting of concentration

The concentration-dependent diffusion-induced electric potential gives rise to variations in the effective diffusivities of the ion species. Table 1 presents the effective diffusivities for different mass ratios of the second and first ion species  $\int_{-\infty}^{\infty} c_2 dx / \int_{-\infty}^{\infty} c_1 dx$  with fixed physical parameters:  $\kappa_1 = 1$ ,  $\kappa_2 = 0.1$ ,  $\kappa_3 = 1$ ,  $z_1 = 1$ ,  $z_2 = 1$ , and  $z_3 = -2$ , and two different Péclet numbers,  $Pe = 0$  and 2. The table shows the triplet of effective diffusivities ( $\kappa_{\text{eff},1}, \kappa_{\text{eff},2}, \kappa_{\text{eff},3}$ ) vary widely, as the mass ratio increases from 0.01 to 100.

As the mass ratio of the second and first ion species decreases to zero, the solution becomes dominated by the first and third ion species, and the effective diffusivity can be

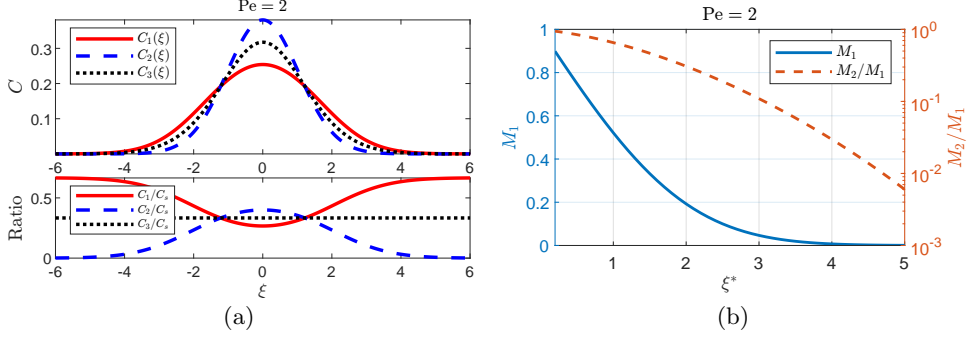


FIGURE 8. (a) The upper panel shows self-similarity solution of the effective equation with the parameters  $Pe = 2$ ,  $\kappa_1 = 1$ ,  $\kappa_2 = 0.1$ ,  $\kappa_3 = 1$ ,  $z_1 = 1$ ,  $z_2 = 1$ , and  $z_3 = -2$ . The lower panel shows the ratio of each component,  $C_i / \sum_{i=1}^3 C_i$ . The lower panel plots the infinity norm of  $\partial_\tau \mathbf{C}(\xi, \tau)$  as a function of  $\tau$ . (b) The blue solid curve represents  $M_1(\xi^*)$  and associate with the left y axis. The red dashed curve represents  $M_2(\xi^*)/M_1(\xi^*)$  and associate with the right y axis.

	Ratio	0.01	0.1	0.5	1	2	10	100
Pe = 0	$\kappa_{\text{eff},1}$	1.00297	1.02772	1.10914	1.1774	1.26774	1.5464	2.0527
	$\kappa_{\text{eff},2}$	0.100359	0.103251	0.111673	0.117514	0.12373	0.13505	0.14135
	$\kappa_{\text{eff},3}$	0.994038	0.943682	0.776652	0.647457	0.50507	0.26336	0.16028
Pe = 2	$\kappa_{\text{eff},1}$	1.05214	1.06501	1.11424	1.16179	1.22965	1.44014	1.74591
	$\kappa_{\text{eff},2}$	0.605669	0.598014	0.57506	0.558975	0.542145	0.513617	0.500019
	$\kappa_{\text{eff},3}$	1.04772	1.02256	0.93452	0.860384	0.771314	0.597846	0.512355

TABLE 1. Effective diffusivity for different mass ratios of the second and first ion species  $\int_{-\infty}^{\infty} c_2 dx / \int_{-\infty}^{\infty} c_1 dx$ . The parameters are  $\kappa_1 = 1$ ,  $\kappa_2 = 0.1$ ,  $\kappa_3 = 1$ ,  $z_1 = 1$ ,  $z_2 = 1$ ,  $z_3 = -2$ .

calculated using the formula for binary electrolytes in equation (4.1),

$$\kappa_{\text{eff},1} = \kappa_{\text{eff},3} = \frac{\kappa_1 \kappa_3 (z_1 - z_3)}{\kappa_1 z_1 - \kappa_3 z_3} + \frac{Pe^2}{8\pi^2} \frac{\kappa_1 z_1 - \kappa_3 z_3}{\kappa_1 \kappa_3 (z_1 - z_3)} = 1 + \frac{1}{2\pi^2} \approx 1.05066. \quad (4.3)$$

As shown previously in figure 7 and 8, for these physical parameters,  $c_1$  is much larger than  $c_2$  for large  $x$ . Therefore, the mass ratio of the second and first ion species decreasing to zero implies that  $c_2/c_1 \rightarrow 0$  for all  $x$ . As a result, the diffusion tensor  $\mathbf{D} + Pe^2 \mathbf{D}^{-1}$  provided in (4.2) becomes

$$\begin{bmatrix} \frac{\kappa_1 \kappa_3 (z_1 - z_3)}{\kappa_1 z_1 - \kappa_3 z_3} + \frac{Pe^2}{8\pi^2} \frac{\kappa_1 z_1 - \kappa_3 z_3}{\kappa_1 \kappa_3 (z_1 - z_3)} & \frac{Pe^2}{8\pi^2} \frac{(\kappa_2 - \kappa_3) z_2}{\kappa_2 \kappa_3 (z_1 - z_3)} - \frac{\kappa_1 (\kappa_2 - \kappa_3) z_2}{\kappa_1 z_1 - \kappa_3 z_3} \\ 0 & \kappa_2 + \frac{Pe^2}{8\pi^2 \kappa_2} \end{bmatrix}. \quad (4.4)$$

Therefore, the formula of  $\kappa_{\text{eff},2}$  remains the same as the formula in classical Taylor dispersion (3.33)

$$\kappa_{\text{eff},2} = \kappa_2 + \frac{Pe^2}{8\pi^2 \kappa_2} = \frac{1}{10} + \frac{5}{\pi^2} \approx 0.606606, \quad (4.5)$$

which suggests that when the concentration of the second ion species is much smaller

than that of the first and third ion species, the second ion species can be considered as passively advected by the shear flow and is decoupled from the first and third ion species.

In the opposite limit, where the mass ratio of the second and first ion species tends to infinity, the effective diffusivities of the second and third ion species converge to

$$\kappa_{\text{eff},2} = \kappa_{\text{eff},3} = \frac{\kappa_2 \kappa_3 (z_2 - z_3)}{\kappa_2 z_2 - \kappa_3 z_3} + \frac{\text{Pe}^2}{8\pi^2} \frac{\kappa_2 z_2 - \kappa_3 z_3}{\kappa_2 \kappa_3 (z_2 - z_3)} = \frac{1}{7} + \frac{7}{2\pi^2} \approx 0.497481, \quad (4.6)$$

which is consistent with the formula for binary electrolytes in equation (4.1). Although we may except the first ion species still follows the formula of the Taylor dispersion,  $\kappa_{\text{eff},1} = \kappa_1 + \frac{\text{Pe}^2}{8\pi^2 \kappa_1} = 1 + \frac{1}{2\pi^2} \approx 1.05066$ , is inconsistent with the value presented in table 1. The reason is that the limit  $\int_{-\infty}^{\infty} c_2 dx / \int_{-\infty}^{\infty} c_1 dx \rightarrow \infty$  does not necessarily imply  $c_2/c_1 \rightarrow \infty$ , and the conditions for the previous asymptotic analysis are not valid. Due to the nonlinearity of the problem, it is difficult to find a closed-form expression for  $\kappa_{\text{eff},1}$  in this limit.

The classical theory of Taylor dispersion has been used to study the effective diffusivity of a solute in a channel, taking into account factors such as molecular diffusivity, channel cross-sectional geometry, and flow rate. Using the measured effective diffusivities, the molecular diffusivity can be easily calculated by determining the geometry factor and flow rate. This technique has been widely used for diffusivity measurement (Bello *et al.* (1994); Taladriz-Blanco *et al.* (2019); Leaist (2017)). However, as we have demonstrated in this section for a multispecies electrolyte solution, the effective diffusivity is also dependent on the concentration ratio of the components. This finding suggests that the Taylor dispersion method can be used to identify the relative concentrations of the components in a multispecies electrolyte mixture.

## 5. Conclusion and discussion

The effective equation of multispecies electrolyte solutions arising from the interplay of the shear flow advection and ion-electric interaction in the channel domain is studied theoretically and numerically in this paper.

Using homogenization methods, we have derived an effective equation that depends only on the longitudinal variable of the channel at the diffusion time scale. Our analysis of the effective equation shows that the concentration distribution's variance asymptotically grows linearly in time, and we have demonstrated that the effective equation has a reciprocal property. That is, the system without flow is equivalent to the system with a strong flow and scaled physical parameters.

We averaged the advection-Nernst-Planck equation in the transverse direction of the channel domain using the homogenization method at the diffusion time scale, which results in an effective equation that depends only on the longitudinal variable of the channel. The analysis of the effective equation shows that the variance of the concentration distribution asymptotically grows linearly in time, and the self-similar solution of the effective equation may be used to calculate the effective diffusivity. We show that the effective equation has the property that the flow-free system is asymptotically equivalent to the system with a strong flow and scaled physical parameters. Last, we have shown that the nonlinear effective equation can be approximated by a diffusion equation when the background concentration is nonzero, leading to a formula for measuring the mutual diffusion coefficients.

In addition to the analytical results, to validate our analytical findings, we have

conducted numerical simulations, which reveal several interesting properties arising from the nonlinearity of the advection-Nernst-Planck equation. Firstly, we observe that ion-electric interaction can dominate over shear flow, resulting in some species moving in the opposite direction of the shear flow. Secondly, different ion species can separate at the early stage or at the diffusion time scale, and the degree of separation can be increased or decreased by the shear flow, depending on the physical parameters. Thirdly, effective diffusivity can be a non-monotonic function of the Péclet number, in contrast to Taylor dispersion where the effective diffusivity monotonically increases with the Péclet number. Fourth, when the initial conditions belong to different types, even if the physical parameters and mass ratio are the same, the resulting effective diffusivity can be different. Fifth, even with the Gaussian initial condition, the longitudinal distribution of the concentration can have a highly non-Gaussian shape and may not be unimodal. Fifth, the relationship between effective diffusivity and concentration offers a method to calculate the ratio of each component's concentrations.

The future study includes several directions. Firstly, while we mainly focused on solutions with three ion species in our numerical simulations, it would be interesting to extend the study to solutions with more components. Secondly, the current study only considers straight channel domains, but the inclusion of curved boundaries would provide insight into many practical applications such as manufacturing a passive mixer for microchannels (Stone *et al.* (2004); Stroock *et al.* (2002); Ajdari *et al.* (2006); Oevreeide *et al.* (2020)), modeling the fluid flows over rough surfaces Carney & Engquist (2022), analyzing solute transport in river (Fischer (1969); Smith (1983); Yotsukura & Sayre (1976)), modeling blood vessel (Marbach & Alim (2019)). Lastly, while our study considers the scalar passively advected by the fluid flow, future research could explore the full coupling of the ion-electric interaction with the fluid equation, providing a more comprehensive understanding of the system's behavior.

## 6. Acknowledgements

I would like to acknowledge the inspiration for this study provided by Robert Hunt, who brought by the paper (Gupta *et al.* (2019)) to my attention, and by my advisor Professor McLaughlin, whose guidance on the project (Ding *et al.* (2021)) was invaluable.

## Appendix A. Effective equation for some shear flows

This section presents explicit expression of the coefficient  $\langle u \Delta_{\mathbf{y}}^{-1} u \rangle_{\mathbf{y}, \tau}$  in equation (3.18) for some classical flows and the flow used in the numerical simulation.

The inversion of the Laplace operator in equation (3.18) depends on the domain geometry. In the parallel-plate channel domain,  $\Omega = \{y | y \in [0, 1]\}$ , the formula is

$$\Delta^{-1} u = \int_0^y \int_0^{s_2} u(s_1) ds_1 ds_2. \quad (\text{A } 1)$$

In the pipe geometry,  $\Omega = \{\mathbf{y} | |\mathbf{y}| \leq 1\}$ , the formula for an axisymmetric function  $u(r)$ ,  $r = |\mathbf{y}|$  is

$$\Delta^{-1} u = \int_0^r \frac{1}{s_2} \int_0^{s_2} s_1 u(s_1) ds_1 ds_2. \quad (\text{A } 2)$$

In the parallel-plate channel domain, the non-dimensionalized pressure-driven shear

flow is  $u = 4(1 - y)y$ , where the characteristic velocity is selected to be the maximum velocity. To use the conclusion in section 3.1, one have to make a Galilean translation in the  $x$ -direction as mentioned earlier, so that the average shear over the transverse plane has mean zero. The shear flow in the new frame of reference is  $u = 4((1 - y)y + \frac{1}{6})$ . With this expression, equation (3.18) becomes

$$\partial_t \mathbf{c}_0 = \partial_x \left( \left( \mathbf{D} + \frac{2\text{Pe}^2}{945} \mathbf{D}^{-1} \right) \partial_x \mathbf{c}_0 \right). \quad (\text{A } 3)$$

The simulation uses a simpler shear flow profile  $u(y) = \cos(2\pi y)$ . The corresponding effective equation is

$$\partial_t \mathbf{c}_0 = \partial_x \left( \left( \mathbf{D} + \frac{\text{Pe}^2}{8\pi^2} \mathbf{D}^{-1} \right) \partial_x \mathbf{c}_0 \right). \quad (\text{A } 4)$$

In the pipe geometry, the non-dimensionalized pressure-driven shear flow in the mean velocity frame of reference is  $u = \frac{1}{2} - r^2$ ,  $r = |\mathbf{y}|$ . With this expression, equation (3.18) becomes

$$\partial_t \mathbf{c}_0 = \partial_x \left( \left( \mathbf{D} + \frac{\text{Pe}^2}{192} \mathbf{D}^{-1} \right) \partial_x \mathbf{c}_0 \right). \quad (\text{A } 5)$$

## REFERENCES

- AJDARI, ARMAND, BONToux, NATHALIE & STONE, HOWARD A 2006 Hydrodynamic dispersion in shallow microchannels: the effect of cross-sectional shape. *Analytical Chemistry* **78** (2), 387–392.
- AMINIAN, MANUCHEHR, BERNARDI, FRANCESCA, CAMASSA, ROBERTO, HARRIS, DANIEL M & McLAUGHLIN, RICHARD M 2016 How boundaries shape chemical delivery in microfluidics. *Science* **354** (6317), 1252–1256.
- AMINIAN, MANUCHEHR, BERNARDI, FRANCESCA, CAMASSA, ROBERTO, HARRIS, DANIEL M & McLAUGHLIN, RICHARD M 2018 The diffusion of passive tracers in laminar shear flow. *JoVE (Journal of Visualized Experiments)* (135), e57205.
- AMINIAN, MANUCHEHR, BERNARDI, FRANCESCA, CAMASSA, ROBERTO & McLAUGHLIN, RICHARD M 2015 Squaring the circle: Geometric skewness and symmetry breaking for passive scalar transport in ducts and pipes. *Physical review letters* **115** (15), 154503.
- ARIS, RUTHERFORD 1956 On the dispersion of a solute in a fluid flowing through a tube. *Proceedings of the Royal Society of London. Series A. Mathematical and Physical Sciences* **235** (1200), 67–77.
- ARIS, R 1960 On the dispersion of a solute in pulsating flow through a tube. *Proceedings of the Royal Society of London. Series A. Mathematical and Physical Sciences* **259** (1298), 370–376.
- AULT, JESSE T, WARREN, PATRICK B, SHIN, SANGWOO & STONE, HOWARD A 2017 Diffusiophoresis in one-dimensional solute gradients. *Soft matter* **13** (47), 9015–9023.
- BARENBLATT, GRIGORY ISAAKOVICH & ISAAKOVICH, BARENBLATT GRIGORY 1996 *Scaling, self-similarity, and intermediate asymptotics: dimensional analysis and intermediate asymptotics*. Cambridge University Press.
- BELLO, MICHAEL S, REZZONICO, ROBERTA & RIGHETTI, PIER GIORGIO 1994 Use of Taylor-Aris dispersion for measurement of a solute diffusion coefficient in thin capillaries. *Science* **266** (5186), 773–776.
- BEN-YAAKOV, S 1972 Diffusion of sea water ions-i. diffusion of sea water into a dilute solution. *Geochimica et Cosmochimica Acta* **36** (12), 1395–1406.
- BHATTACHARYYA, SOMNATH, GOPMANDAL, PARTHA P, BAIER, TOBIAS & HARDT, STEFFEN 2013 Sample dispersion in isotachopheresis with poiseuille counterflow. *Physics of Fluids* **25** (2), 022001.
- BOUDREAU, BERNARD P, MEYSMAN, FILIP JR & MIDDELBURG, JACK J 2004 Multicomponent ionic diffusion in porewaters: Coulombic effects revisited. *Earth and Planetary Science Letters* **222** (2), 653–666.

- BRONSKI, JARED C, DING, LINGYUN & MCLAUGHLIN, RICHARD M 2022 Correlation function of a random scalar field evolving with a rapidly fluctuating gaussian process. *arXiv preprint arXiv:2202.11223* .
- CAMASSA, ROBERTO, LIN, ZHI & MCLAUGHLIN, RICHARD M 2010 The exact evolution of the scalar variance in pipe and channel flow. *Communications in Mathematical Sciences* **8** (2), 601–626.
- CARNEY, SEAN P & ENGQUIST, BJÖRN 2022 Heterogeneous multiscale methods for rough-wall laminar viscous flow. *Communications in Mathematical Sciences* **20** (8), 2069–2106.
- CASALINI, TOMMASO, SALVALAGLIO, MATTEO, PERALE, GIUSEPPE, MASI, MAURIZIO & CAVALLOTTI, CARLO 2011 Diffusion and aggregation of sodium fluorescein in aqueous solutions. *The Journal of Physical Chemistry B* **115** (44), 12896–12904.
- CHATWIN, PC 1970 The approach to normality of the concentration distribution of a solute in a solvent flowing along a straight pipe. *Journal of Fluid Mechanics* **43** (2), 321–352.
- CHATWIN, PC 1975 On the longitudinal dispersion of passive contaminant in oscillatory flows in tubes. *Journal of Fluid Mechanics* **71** (3), 513–527.
- DEEN, WILLIAM MURRAY 1998 *Analysis of transport phenomena*, , vol. 2. Oxford university press New York.
- DING, LINGYUN, HUNT, ROBERT, MCLAUGHLIN, RICHARD M & WOODIE, HUNTER 2021 Enhanced diffusivity and skewness of a diffusing tracer in the presence of an oscillating wall. *Research in the Mathematical Sciences* **8** (3), 1–29.
- DING, LINGYUN & MCLAUGHLIN, RICHARD M 2021 Ergodicity and invariant measures for a diffusing passive scalar advected by a random channel shear flow and the connection between the Kraichnan-Majda model and Taylor-Aris dispersion. *Physica D: Nonlinear Phenomena* p. 133118.
- DING, LINGYUN & MCLAUGHLIN, RICHARD M 2022 Determinism and invariant measures for diffusing passive scalars advected by unsteady random shear flows. *Physical Review Fluids* **7** (7), 074502.
- DUTTA, DEBASHIS & LEIGHTON, DAVID T 2001 Dispersion reduction in pressure-driven flow through microetched channels. *Analytical chemistry* **73** (3), 504–513.
- EGGERS, JENS & FONTELOS, MARCO A 2008 The role of self-similarity in singularities of partial differential equations. *Nonlinearity* **22** (1), R1.
- FISCHER, HUGO B 1969 The effect of bends on dispersion in streams. *Water resources research* **5** (2), 496–506.
- GANOR, NETHANEL, RUBIN, SHIMON & BERCOVICI, MORAN 2015 Diffusion dependent focusing regimes in peak mode counterflow isotachophoresis. *Physics of Fluids* **27** (7), 072003.
- GOPMANDAL, PARTHA P & BHATTACHARYYA, S 2015 Effects of convection on isotachophoresis of electrolytes. *Journal of fluids engineering* **137** (8).
- GUPTA, ANKUR, SHIM, SUIN, ISSAH, LUQMAN, MCKENZIE, CAMERON & STONE, HOWARD A 2019 Diffusion of multiple electrolytes cannot be treated independently: model predictions with experimental validation. *Soft Matter* **15** (48), 9965–9973.
- HOSOKAWA, YOSHIFUMI, YAMADA, KAZUO, JOHANNESSON, BJÖRN & NILSSON, LARS-OLOF 2011 Development of a multi-species mass transport model for concrete with account to thermodynamic phase equilibriums. *Materials and Structures* **44**, 1577–1592.
- LEAIST, DEREK G 2017 Quinary mutual diffusion coefficients of aqueous mannitol+ glycine+ urea+ kcl and aqueous tetrabutylammonium chloride+ licl+ kcl+ hcl solutions measured by taylor dispersion. *Journal of Solution Chemistry* **46** (4), 798–814.
- LEAIST, DEREK G & HAO, LING 1993 Diffusion in buffered protein solutions: combined nernst-planck and multicomponent fick equations. *Journal of the Chemical Society, Faraday Transactions* **89** (15), 2775–2782.
- LEAIST, DEREK G & MACEWAN, KIMBERLEY 2001 Coupled diffusion of mixed ionic micelles in aqueous sodium dodecyl sulfate+ sodium octanoate solutions. *The Journal of Physical Chemistry B* **105** (3), 690–695.
- LEE, GARAM, LUNER, ALAN, MARZUOLA, JEREMY & HARRIS, DANIEL M 2021 Dispersion control in pressure-driven flow through bowed rectangular microchannels. *Microfluidics and Nanofluidics* **25** (4), 1–11.
- LIU, CHONGXUAN, SHANG, JIANYING & ZACHARA, JOHN M 2011 Multispecies diffusion models: A study of uranyl species diffusion. *Water Resources Research* **47** (12).

- MAEX, REINOUD 2013 *Nernst-Planck Equation*, pp. 1–7. New York, NY: Springer New York.
- MARBACH, SOPHIE & ALIM, KAREN 2019 Active control of dispersion within a channel with flow and pulsating walls. *Physical Review Fluids* **4** (11), 114202.
- NGO-CONG, D, MOHAMMED, FJ, STRUNIN, DV, SKVORTSOV, AT, MAI-DUY, N & TRAN-CONG, T 2015 Higher-order approximation of contaminant transport equation for turbulent channel flows based on centre manifolds and its numerical solution. *Journal of Hydrology* **525**, 87–101.
- OEVRÉEIDE, INGRID H, ZOELLNER, ANDREAS, MIELNIK, MICHAL M & STOKKE, BJØRN T 2020 Curved passive mixing structures: a robust design to obtain efficient mixing and mass transfer in microfluidic channels. *Journal of Micromechanics and Microengineering* **31** (1), 015006.
- POISSON, A & PAPAUD, A 1983 Diffusion coefficients of major ions in seawater. *Marine Chemistry* **13** (4), 265–280.
- PRICE, WILLIAM E 1988 Theory of the Taylor dispersion technique for three-component-system diffusion measurements. *Journal of the Chemical Society, Faraday Transactions 1: Physical Chemistry in Condensed Phases* **84** (7), 2431–2439.
- RIBEIRO, ANA CF, BARROS, MARISA CF, VERISSIMO, LUIS MP, ESTESO, MIGUEL A & LEAIST, DEREK G 2019 Coupled mutual diffusion in aqueous sodium (salicylate+ sodium chloride) solutions at 25 c. *The Journal of Chemical Thermodynamics* **138**, 282–287.
- RODRIGO, M MELIA, ESTESO, MIGUEL A, RIBEIRO, ANA CF, VALENTE, AJM, CABRAL, ANA MTDPV, VERISSIMO, LUIS MP, MUSILOVA, L, MRACEK, A & LEAIST, DEREK G 2021 Coupled mutual diffusion in aqueous paracetamol+ sodium hydroxide solutions. *Journal of Molecular Liquids* **334**, 116216.
- RODRIGO, M MELIA, VALENTE, ARTUR JM, ESTESO, MIGUEL A, CABRAL, ANA MTDPV & RIBEIRO, ANA CF 2022 Ternary diffusion in aqueous sodium salicylate+ sodium dodecyl sulfate solutions. *The Journal of Chemical Thermodynamics* **174**, 106859.
- SHERMAN, JACK & MORRISON, WINIFRED J 1950 Adjustment of an inverse matrix corresponding to a change in one element of a given matrix. *The Annals of Mathematical Statistics* **21**, 124–127.
- SMITH, GR & SANSOM, MSP 1998 Dynamic properties of  $\text{Na}^+$  ions in models of ion channels: a molecular dynamics study. *Biophysical Journal* **75** (6), 2767–2782.
- SMITH, RONALD 1982 Contaminant dispersion in oscillatory flows. *Journal of Fluid Mechanics* **114**, 379–398.
- SMITH, RONALD 1983 Longitudinal dispersion coefficients for varying channels. *Journal of Fluid Mechanics* **130**, 299–314.
- STONE, HOWARD A, STROOCK, ABRAHAM D & AJDARI, ARMAND 2004 Engineering flows in small devices: microfluidics toward a lab-on-a-chip. *Annu. Rev. Fluid Mech.* **36**, 381–411.
- STROOCK, ABRAHAM D, DERTINGER, STEPHAN KW, AJDARI, ARMAND, MEZIC, IGOR, STONE, HOWARD A & WHITESIDES, GEORGE M 2002 Chaotic mixer for microchannels. *Science* **295** (5555), 647–651.
- TABRIZINEJADAS, SARA, CARRAYROU, JEROME, SAALTINK, MAARTEN W, BAALOUSHA, HUSAM MUSA & FAHS, MARWAN 2021 On the validity of the null current assumption for modeling sorptive reactive transport and electro-diffusion in porous media. *Water* **13** (16), 2221.
- TALADRIZ-BLANCO, PATRICIA, ROTHEN-RUTISHAUSER, BARBARA, PETRI-FINK, ALKE & BALOG, SANDOR 2019 Precision of Taylor dispersion. *Analytical Chemistry* **91** (15), 9946–9951.
- TAYLOR, GEOFFREY INGRAM 1953 Dispersion of soluble matter in solvent flowing slowly through a tube. *Proceedings of the Royal Society of London. Series A. Mathematical and Physical Sciences* **219** (1137), 186–203.
- TAYLOR, MICHAEL 2012 Random walks, random flows, and enhanced diffusivity in advection-diffusion equations. *Discrete & Continuous Dynamical Systems-B* **17** (4), 1261.
- TOURNASSAT, CHRISTOPHE, STEEFEL, CARL I & GIMMI, THOMAS 2020 Solving the Nernst-Planck equation in heterogeneous porous media with finite volume methods: Averaging approaches at interfaces. *Water Resources Research* **56** (3), e2019WR026832.
- VEDEL, SØREN & BRUUS, HENRIK 2012 Transient Taylor–Aris dispersion for time-dependent flows in straight channels. *Journal of Fluid Mechanics* **691**, 95–122.

- WANG, WEI & ROBERTS, ANTHONY J 2013 Self-similarity and attraction in stochastic nonlinear reaction-diffusion systems. *SIAM Journal on Applied Dynamical Systems* **12** (1), 450–486.
- WU, ZI & CHEN, GQ 2014 Approach to transverse uniformity of concentration distribution of a solute in a solvent flowing along a straight pipe. *Journal of Fluid Mechanics* **740**, 196–213.
- YOTSUKURA, NOBUHIRO & SAYRE, WILLIAM W 1976 Transverse mixing in natural channels. *Water Resources Research* **12** (4), 695–704.
- YOUNG, WR A & JONES, SCOTT 1991 Shear dispersion. *Physics of Fluids A: Fluid Dynamics* **3** (5), 1087–1101.
- YUAN-HUI, LI & GREGORY, SANDRA 1974 Diffusion of ions in sea water and in deep-sea sediments. *Geochimica et cosmochimica acta* **38** (5), 703–714.